REPORT DOCUMENTATION PAGE

Form Approved
OMB No. 0704-0188

1. REPORT DATE *(DD-MM-YYYY)*	2. REPORT TYPE	3. DATES COVERED *(From - To)*
	Technical Paper	

4. TITLE AND SUBTITLE

5a. CONTRACT NUMBER

5b. GRANT NUMBER

5c. PROGRAM ELEMENT NUMBER
62500F

6. AUTHOR(S)

5d. PROJECT NUMBER
2308

5e. TASK NUMBER
M4S7

5f. WORK UNIT NUMBER
345382

7. PERFORMING ORGANIZATION NAME(S) AND ADDRESS(ES)

8. PERFORMING ORGANIZATION REPORT

9. SPONSORING / MONITORING AGENCY NAME(S) AND ADDRESS(ES)

Air Force Research Laboratory (AFMC)
AFRL/PRS
5 Pollux Drive.
Edwards AFB CA 93524-7048

10. SPONSOR/MONITOR'S ACRONYM(S)
XC

11. SPONSOR/MONITOR'S NUMBER(S)

12. DISTRIBUTION / AVAILABILITY STATEMENT

Approved for public release; distribution unlimited.

13. SUPPLEMENTARY NOTES

See attached 8 papers, all with the information on this page.

14. ABSTRACT

15. SUBJECT TERMS

16. SECURITY CLASSIFICATION OF:			17. LIMITATION OF ABSTRACT	18. NUMBER OF PAGES	19a. NAME OF RESPONSIBLE PERSON
a. REPORT	b. ABSTRACT	c. THIS PAGE			Kenette Gfeller
Unclassified	Unclassified	Unclassified	A		19b. TELEPHONE NUMBER *(include area code)* (661) 275-5016

IEPC-95-28

LASER INDUCED FLUORESCENCE OF GROUND STATE HYDROGEN ATOMS IN AN ARCJET PLUME

Jeffrey A. Pobst*, Ingrid J. Wysong**
Hughes STX
Propulsion Directorate
OL-AC Phillips Laboratory
Edwards AFB, CA 93524

Ronald A. Spores†
Propulsion Directorate
OL-AC Phillips Laboratory
Edwards AFB, CA 93524

Abstract

We report two photon laser induced fluorescence measurements near the nozzle exit and in the plume of a 1 kW arcjet thruster. Atomic hydrogen number densities, axial and radial velocities, and translational temperatures are measured in the expansion plume of a 1 kW arcjet operating on hydrogen propellant. Data from recent computational models are compared with the atomic hydrogen density measurements.

Introduction

Arcjets are expected to play an ever increasing role in satellite propulsion needs, primarily for stationkeeping and on-orbit maneuvering in the near term. While the technology is considered viable enough to be deployed on a Telstar IV communications satellite for stationkeeping,[1] arcjet technology is far from maturity. In order to compete successfully with chemical propulsion systems for on-orbit missions, further improvements in arcjet propulsion systems are still required.[2] If needed improvements in the performance level and efficiency of arcjets are to be achieved, an increased understanding of the fundamental physical processes that govern the operation of an arcjet is essential. In addition, an ability to predict the plume behavior of a space propulsion device is necessary for prediction and amelioration of spacecraft interactions.

* Scientist
** Principal Scientist
† Research Engineer

Significant arcjet energy loss results from velocity profile losses due to thick internal boundary layers in the arcjet nozzle and from frozen flow losses such as molecular dissociation. To quantify profile losses, both gas velocity and density distributions must be known. In addition, arcjet models, which are necessary for timely and cost-effective improvements to design, must be tested by comparison with key physical parameters.

At present, only limited inroads have been made into the problem of plume density measurements. For hydrogen arcjet thrusters, determination of species density has previously only been accomplished through a few diagnostic techniques.

Our previous work using multi-photon laser induced fluorescence (LIF) provided the first measurement of ground state hydrogen in an arcjet plume.[3] Atomic hydrogen density profiles were reported near nozzle exit and a preliminary calibration was performed to convert the relative density profiles to absolute number densities.

Knowledge of the atomic density profile at nozzle exit is important for evaluating our understanding of the physical processes in the arcjet thruster and the

computational models that have been written to describe these processes.[4-9] The density of atoms relative to the density of molecules is an indication of how much energy is lost into dissociation of the hydrogen molecules and not recovered through recombination into translational kinetic modes.

To determine the molecular dissociation fraction, the molecular species density needs to be known as well as the atomic number density. The recent use of Raman spectroscopy[10,11] in an arcjet plume has provided the first information on molecular hydrogen densities at the arcjet nozzle plane.

In addition to LIF on the ground state atoms, other absorption spectroscopy techniques[12,13] have been used on arcjet plumes to characterize hydrogen atom densities. These VUV and XUV spectroscopy approaches are quite difficult to implement in practice and are limited to determination of line-of-sight averaged number densities at downstream locations in the plume where the optical depth is not too high.

For measuring velocity and temperature, both ground state LIF[3] and excited state LIF [4,14,15] have proven to be accurate and essentially nonintrusive. Though the excited states of hydrogen are more accessible, most atoms in the plume region are expected to be in the ground state. These two types of LIF temperature and velocity measurements allow examination of the differences between the excited state and ground state species in the non-equilibrium plume environment.

Experiment

This work is performed using two-photon LIF (2PLIF) on ground-state hydrogen atoms in the plume of a 1-kW-class hydrogen arcjet. Since any propellant gas is opaque for the VUV radiation required for single-photon excitation of ground state atoms, 2PLIF at correspondingly longer wavelengths is preferred. The diagnostic technique, which has been developed primarily for use in flames,[16,17,18] uses two photons at 205 nm to promote the atoms from the n=1 to the n=3 electronic state (the Lβ transition). Subsequent 3-2 fluorescence is observed (the Hα transition), as indicated in the energy level diagram in Figure 1.

The apparatus is shown schematically in Figure 2. The laser is a pulsed dye laser pumped by a Nd:YAG with a repetition rate of 10 Hz and a pulse width of 6 ns. The dye laser output at 615 nm is frequency tripled to achieve about 0.5 mJ per pulse at 205 nm. A mirror turns about 80% of the beam toward the arcjet chamber through a variable attenuator placed in the beam, the remaining 20% of beam energy is directed toward a microwave-discharge source of atomic hydrogen.

For axial velocity measurements, the beam is sent directly down the axis of the arcjet flow (Path 1) and is focused with a telescope lens configuration (not shown) outside the chamber with a focal length on the order of 2 m. For radial measurements, the unfocussed beam is sent to a turning prism inside the chamber located underneath the arcjet (Path 2), directed to pass vertically through the plume, and is focused by a 200 mm lens. The laser beam and optics remain fixed, while the arcjet is mounted on a motion control x, y, z stage to translate it for probing different regions of the plume.

A filtered photomultiplier tube (PMT) is placed behind the final turning mirror before the chamber in order to detect amplified spontaneous emission (ASE) that may propagate back along the laser beam path (see further discussion below). A 200 mm focal length, 2" diameter lens is placed inside the chamber to collimate the LIF that is emitted toward the side window. The light is collected outside the chamber, focused through a 1 mm aperture, and detected with a filtered, gated PMT. Since the LIF occurs at 656 nm, the filters used are a 656 nm bandpass interference filter and an RG 645 color glass filter (thus all scattered laser light (205nm) is filtered out). The gated PMT is an ordinary Hamamatsu 928 tube with a special socket that is triggered to detect light for 2 μs during each laser pulse and is off between pulses. This is an important feature that allows us to operate the PMT at full voltage without exceeding the anode current limit due to the bright arcjet emission background. Saturation is avoided by setting the voltage level so that both average current and peak current during the gate remain below the maximum specified for the PMT. A gated integrator with a 30 ns gate is used to amplify and average the Hα fluorescence seen by the PMT. Alternatively, the PMT signal can be digitized by a fast oscilloscope to obtain fluorescence lifetimes and quenching information.

The weak UV beam that is sent into the discharge cell is focused with a 150 mm lens. The cell is run with a slow flow of a few Torr of helium carrier gas and a few percent hydrogen. The LIF is detected through a filtered (ungated) PMT. Simultaneous detection of LIF from the cell during each spectral scan of the arcjet LIF provides a zero-velocity comparison from which to measure Doppler shifts. This discharge cell provides wavelength calibration but not density calibration. A separate discharge cell is used for density calibration inside the chamber when the arcjet is not operating.

The procedure for obtaining absolute number density is based on a method reported by Meier et al.[18,19,20] After a relative number density scan and corresponding lifetime data are taken, the arcjet is turned off and translated away from the collection volume, the chamber is opened, and a second calibration cell is placed in the detection volume with the laser beam passing through it. The LIF signal and lifetime is measured for the hydrogen atoms present in the cell. Atoms are present due to the flow of hydrogen gas through a microwave discharge prior to entering the cell. Since the laser beam, detection optics and electronics have remained the same, the LIF from the arcjet and from the cell will have the same proportionality to absolute number density after correcting for any differences in quenching:

$$N_H^A = \frac{S^A}{S^C} \cdot N_H^C \cdot C_Q$$

S^A and S^C are the signal sizes (integrated over the entire spectral width) from the arcjet and the cell, N_H^A and N_H^C are the absolute number densities of atomic hydrogen in the arcjet and the cell, and C_Q is the scaling factor for the difference in quenching. C_Q is given by the ratio of fluorescence decay rate in the arcjet to that in the calibration cell.

The absolute number density of hydrogen atoms in the discharge cell is obtained using a standard chemical titration method. A schematic of the calibration cell used for this method is shown in Figure 3. The cell is made out of glass tubing and is approximately 30 cm (12 in.) long and 5 cm (2 in.) in diameter. Important to the design of the cell is the long drift tube area with a Teflon tubing liner to reduce gas/wall interactions. This drift tube allows complete mixing of the titration gas and the gas of interest. In this case, the titration gas is NO_2 and H is the gas to be calibrated.

The hydrogen (with a helium carrier gas) enters the drift tube area near one end after passing through a microwave discharge. A dilute mixture of NO_2 in helium is added to the flow through a long thin tube and enters the larger drift tube region at a location past the point where the hydrogen has entered. This reduces the amount of NO_2 that might diffuse upstream and enter the microwave discharge.

The NO_2 reacts rapidly with hydrogen atoms when the two are completely mixed in the large drift tube volume. The calibration involved flowing 1 slpm of a 2% hydrogen in helium mixture and then the addition of 2% NO_2 in helium until the signal decreased, typically at about .08 slpm of NO_2/He. A small vacuum pump brought the cell pressure down to 950 Pa (7.2 Torr) during gas flow.

The LIF signal decreases until it is gone at the point where the partial pressure of added NO_2 is equal to the partial pressure of hydrogen atoms in the cell. Control of the amount of NO_2 added allows the determination of the amount of hydrogen atoms present in the calibration cell. Figure 4 shows data from one calibration run. The NO_2 concentration at the x intercept is equal to the concentration of atomic hydrogen present as each hydrogen atom is reacted away for each NO_2 molecule added in the fast reaction:

$$H + NO_2 \rightarrow OH + NO$$

The large amount of buffer gas and low amount of H significantly reduce possible secondary reactions, making them negligible for the purposes of this experiment. Calibration took place either before or after each arcjet firing, usually on the same day.

All thruster data were taken on a 1-kW-class arcjet designed by NASA Lewis Research Center.[21] The cathode gap was set to 0.07". The arcjet operated at 137V, 10A (1.37 kW) on a hydrogen gas flow of 13.1 mg/s (8.74 slpm) at an operating chamber pressure of 6 Pa (45 mTorr). The gas flow and power were chosen to closely match the conditions under which the most complete set of previous diagnostic data for a 1 kW hydrogen arcjet were taken, in order to facilitate comparisons between different data sets and between data and

models.[10,15,22] A voltage-current curve of our arcjet, was shown in a previous publication.[3] The hydrogen flow controller for the arcjet as well as the flow meters for the discharge cell were calibrated using a wet test meter.

Results and Discussion

Figure 5 shows a sample spectral scan of the hydrogen atom profile from the arcjet and from the discharge cell, taken with an axial laser beam. Each profile is fit to a Gaussian shape using a Levenberg-Marquardt least squares fit[23] and the wavelength shift of the two centers yields the axial velocity, while the width of each Gaussian yields the temperature. A number of possible uncertainties enter into this analysis. A focused pulsed laser beam creates a very high instantaneous energy density, which is needed to excite the two-photon transition, but also may induce other non-linear processes. Multi-photon ionization (MPI) will occur, and partial saturation of the transition becomes possible, even though the two-photon absorption cross section is very small. In addition, amplified spontaneous emission (ASE) will take place, since a population inversion is created between the pumped n=3 level and the nearly empty n=2 level. The population inversion can cause gain to occur for any photon emitted in the forward or backward direction along the laser beam.[24,25,26] If ASE or MPI become large, they become a non-negligible loss mechanism for the LIF process. Saturation will cause power broadening of the Doppler profile of the transition, and saturation, ASE or MPI will cause the power dependence of the LIF signal to deviate from the expected behavior proportional to power squared.

We have performed a power-dependence study, which is summarized in Figure 6 and Figure 7. We find that when the laser beam to the arcjet is attenuated to below 0.03 mJ per pulse for the radial beam, the LIF is proportional to the power squared, as indicated by the slope of 2 on a log-log plot. At these lower laser powers, the ASE signal has fallen away drastically from its large size and does not appear to attenuate the LIF signal. At higher laser powers reduction in LIF signal from the power squared proportionality is observed. In addition, the temperatures measured (shown in Figure 7) appear to increase at higher laser powers where saturation broadening becomes a significant component of the linewidth. At lower powers, the temperature remains constant at its true value.

Figure 8 shows the differences in the lineshape between the measured ASE signal and the measured LIF signal in wavelength space. Due to these differences, compensating for the ASE loss mechanism through measurement of the ASE was deemed unreliable. Efforts were made to operate at laser powers where ASE loss was insignificant and did not cause deviation from the power squared behavior in the LIF signal. The temperature and number density data presented here are all obtained with a laser energy of about 0.03 mJ per pulse. Laser powers lower than this were found to approach signal to noise limits for our configuration, most notably when probing away from the center of the arcjet nozzle.

Another broadening mechanism that is present is Stark broadening of the transition due to the free electrons present in the arcjet plume. We do not have any direct measurement of the profile of the electron number density for our arcjet, but it has been measured for nearly identical conditions[22] to be less than 2×10^{13} cm^{-3} at maximum in the center of the nozzle exit plane. This value of n_e would cause a Stark width of 0.002Å for the Lβ line.[27] A simulated Voigt profile using this Lorentzian width shows that, for a typical measured linewidth of 0.029Å, accounting for the Stark broadening would cause the temperature from the Doppler portion of the linewidth to go down from 1600K to 1490K. This represents the likely maximum uncertainty in our temperature due to Stark broadening, and will be greatest at the center of the nozzle where n_e is largest.

A small amount of line broadening is caused by the linewidth of the dye laser beam which, unlike that of cw ring dye lasers, is non-negligible compared with the atomic linewidth. The laser linewidth at 205 nm has been measured by taking an LIF spectrum of NO gas in the cell. Since NO is much heavier than hydrogen, and is at room temperature, the width of the rotational lines in the LIF spectrum reflect only the linewidth of the laser (as long as care is taken to use unblended rotational lines). This has shown that the laser has a width of 0.28 cm^{-1} or 0.012 Å at 205 nm. The effect of the laser width is taken into account using the following relation:[28]

$$(\Delta\nu)^2 = (\Delta\nu_D + 2\Delta\nu_l)^2$$

where $\Delta\nu_D$ is the true Doppler width of the line (in cm^{-1}), $\Delta\nu_l$ is the width of the laser, $\Delta\nu$ is the measured transition width, and the factor of two is due to the two-photon probe method.

Velocity is measured by observing the Doppler shift of the absorption line and determining the velocity relative to the incoming photons responsible for the shift.

$$v = \frac{\Delta\lambda}{\lambda_0} c$$

where v is the velocity, $\Delta\lambda$ is the wavelength shift, λ_0 is the zero velocity line center, and c is the speed of light. Determining the line center of a profile with the fitting process discussed earlier is relatively simple and quite accurate. The uncertainty from the data analysis is less than the symbol size of the data shown in the following velocity figures.

Figure 9 shows the radial distribution of axial velocities 0.4mm from the arcjet nozzle exit. The velocities were measured with a laser beam entering the plume of the arcjet axially. Figure 10 shows the corresponding distribution of the radial component of velocity when the beam is brought to the plume radially. Data for the plot were taken over several days and the scatter may indicate day to day operational changes in the arcjet as well as measurement and alignment uncertainties. It should be noted that velocity profiles of the ground state hydrogen atoms are in close agreement with previous measurements using excited state LIF.[15]

The profiles are extremely sensitive to centering in both vertical and horizontal directions and an alignment procedure is performed prior to evacuation of the chamber. After arcjet operation commences and a period of heating (approximately 30 minutes to an hour) takes place, sample velocity distributions are taken horizontally and vertically to center the optical detection with the peak velocity of the arcjet plume. This usually requires an adjustment of 0.25 mm to 0.5 mm from the initial alignment at atmosphere in one or both of the axes that make up the nozzle exit plane. The y (axial) axis zero is defined to be where the arcjet nozzle moves into the laser beam and reduces the LIF signal in half. Since the laser is focused to a spot size measured to be .040 mm ±0.01 mm, this position can be set with an uncertainty of at least ±0.1 mm. This is checked periodically to insure that it remains constant. During the initial warming up period of the arcjet, approximately 0.5 mm of expansion is observed in the 1 kW arcjet nozzle.

Figure 11 shows a temperature profile at 0.4 mm from nozzle exit. The results indicate a peak temperature around 1600K - 1800K in the center dropping to 1000K - 1200K over the 5 mm radius of the nozzle exit. The low signal to noise of the fluorescence (when low laser power is used, as described above) makes measurement of the Doppler width difficult, especially at the edges, though Doppler shift measurements are less affected. Temperature is based upon the square of the measured Doppler width and can be written in terms of width in the following manner:[29]

$$\delta\lambda = 7.16\times10^{-7}\lambda_0\sqrt{\frac{T}{M}}$$

where $\delta\lambda$ is the linewidth due to Doppler broadening, λ_0 is the line center, M is the molar mass of the gas, and T is the translational temperature. The constant in the equation is based upon the values of the speed of light and the molecular gas constant.

Substantially greater uncertainty is associated with temperature than with velocity. The uncertainty due to scatter can be seen in the plot, which includes data from several different days.

Figure 12 shows our observed atomic ground state temperature measurements with values taken from published excited state temperature measurements[30] and molecular rotational temperatures.[11] While the temperatures predicted by the ground state hydrogen atoms are quite similar to the rotational molecular temperatures, our temperature measurements of the ground state hydrogen atoms are about a factor of two cooler in the center than those of the excited-state hydrogen atoms, possibly indicating a significant non-equilibrium between the excited state and ground state hydrogen atoms.

The dye laser was tuned to 656 nm in an attempt to directly measure the excited state hydrogen atoms in our arcjet and ensure that the apparent non-equilibrium is real and not due to differences

between our system and Stanford's. The Hα LIF was detected, but the power broadening due to the focused, pulsed laser was very severe. Decreasing the laser power enough to alleviate the power broadening led to an unacceptable signal-to-noise ratio, so this measurement could not be pursued.

Figure 13 shows two sample fluorescence decay curves, one measured at the center of the nozzle exit plane, and the other measured near the edge of the nozzle exit plane. Change in the lifetime represents the effect of collisional quenching in the 3-2 transition. The curves are obtained by digitizing the LIF signal from the PMT using a 500 MHz oscilloscope. Also shown in the figure is a curve from the laser scatter only (with optical filters removed from the PMT) to show the time resolution of the system with no LIF present. Decay curves such as Figure 13 are analyzed by starting at 10 ns after the laser pulse and fitting the signal to an exponential decay.

Figure 14 shows results for lifetime measurements from several separate days as a function of position along the nozzle exit. The lifetimes measured in the arcjet plume indicate the collisional quenching due to electrons, H_2, or most likely some combination of both. The LIF signal is only proportional to number density if it is corrected for losses due to quenching.

The need for correcting for collisional quenching is evident in Figure 15 where the density prediction before and after the correction for quenching is seen. In this case the correction is significant in the center region, and minimal at the edge of the profile.

Figure 16 shows the calibrated number density profile of hydrogen atoms near the exit plane of the nozzle (0.4mm from nozzle exit plane). This is obtained from the area under the curve of the hydrogen atom profile (at low laser power to avoid ASE, MPI and saturation), and corrected by the fluorescence yield at each location. Separately calibrated data sets from many different days are included in the plot. The peak of the density profile is at the center of the nozzle exit plane and indicates a number density of 1×10^{16} cm^{-3} and falls off about one and a half orders of magnitude over the 5 mm to the nozzle exit wall.

Also shown in the figure are the predicted exit plane number density distributions from three arcjet models. The Boyd model is authored by I. D. Boyd at Cornell University.[9] It is a Direct Simulation Monte Carlo (DSMC) particle code that predicts physical properties through most of the arcjet nozzle and out into the plume. The Butler model is authored by G. W. Butler at Olin Aerospace Corporation and is a Navier Stokes (NS) code that computes the flow properties throughout the arcjet nozzle, stopping at the nozzle exit.[5,31] A separate NS code written by Megli, Krier, and Burton from the University of Illinois predicts results that are also shown in the figure.[32] Like the Butler model the calculations extend to the nozzle exit, but not into the plume.

The number density differences between the data and the model indicate almost an order of magnitude higher atomic density than predicted by the two Navier Stokes models and a factor of three higher than the DSMC prediction.

Shown in Table 1 is a comparison of the predictions for both atomic hydrogen and molecular hydrogen densities for each of the models. In addition experimental results on species density from this work and that of Beattie and Cappelli at Stanford University are shown.[11]

Note that the predictions for all three models agree well with each other and with experiment for molecular hydrogen density at the centerline of nozzle exit. As seen in the previous figure, the differences in atomic number density can be quite large. These atomic discrepancies, in light of the molecular density agreements, indicate different molecular dissociation fractions predicted by the codes and by the combination of the two experiments at the center of the nozzle exit.

The two experimental efforts indicate a dissociation fraction as large as 50% at the nozzle exit center. This is an approximation for dissociation as the error bars on both experiments are quite large and the experiments were done on two different arcjets, though every effort was made to operate at similar arcjet conditions.

The predicted dissociation fraction from each of the models is substantially less ranging from 5% to 18% depending upon the model. Accurately predicting the dissociation fraction could be closely related to understanding the amount of frozen flow energy loss

in the arcjet thruster and an important step in improving arcjet efficiency from the current 30% to 35% range.

Figure 16 shows a two dimensional profile of the hydrogen atomic number density data taken at .4 mm downstream of nozzle exit. This figure shows a generally axisymmetric flow with non-smooth features at the edges of each density range. The rough contours are caused partially by the 1/distance algorithm used to create the contours from a Cartesian data set that was large and intensive to take, but still less in quantity of points than perhaps desirable for identifying precise gradients. In addition, the noise in the data as seen in the earlier density plot of Figure 16 is significant and can cause the appearance of shifting gradients in this type of two dimensional representation.

Figure 17 shows the same data in the two dimensional plot all collapsed onto a single axis with radius as the ordinate. Each line is a single "spoke" of the two dimensional data shown in Figure 17. The lines are shown together to illustrate that the spread between the different radial profiles is within the scatter that is seen when examining just one radial profile on several different days. This indicates that the flow appears to be quite axisymmetric within the experimental uncertainty.

Examining the behavior of the density and temperature as the flow exits the nozzle, Figure 19 shows the density and temperature gradients from 0.2mm past nozzle exit to 30 mm downstream along the nozzle centerline. One of the benefits of looking at these trends was to examine the validity of comparing data taken at 0.4 mm downstream to the properties right at nozzle exit. Since the optical data for this experiment could not be observed inside the nozzle, many data points were taken close to the nozzle exit and the axial position axis is shown on a logarithmic scale. Note that while the density does appear to decrease as it exits, the difference between the data taken at 0.4 mm and what would be extrapolated back to nozzle exit is well within the error bars shown in Figure 16, and one expects that the data would not appear significantly different if the exact nozzle exit was able to be probed with this technique. In addition, if the data fails to predict the correct atomic number density right at the nozzle exit, it would appear from the trend in this figure to underpredict the number of hydrogen atoms at nozzle exit leading to an even greater discrepancy with the predictions from the computational models.

Conclusions

Using two-photon LIF, hydrogen ground state number densities, velocities and temperatures have been measured near the arcjet nozzle exit. General agreement with previous nozzle exit velocity distributions is seen, with no effect of translational slip being observed. Temperature measurements of the atomic ground state appear to be significantly cooler than those previously measured in excited states indicating non-equilibrium behavior.

Number density measurements at the nozzle exit are made, carefully avoiding such loss mechanisms as multi-photon ionization, amplified spontaneous emission, and laser saturation. Fluorescence quenching was measured and corrected for.

The number density distributions are compared with computational modeling data and indicate a significantly higher, more peaked number density than predicted. Including recent molecular density data, a higher dissociation fraction is observed than is currently predicted by the computational models indicating that frozen flow energy loss may be a more significant contribution to the arcjet's low efficiency.

Axial symmetry of the density at nozzle exit is observed within the scatter of the measurement and both density and temperature axial trends are observed indicating that data taken at 0.4mm is likely representative of properties right at the nozzle exit and data across the nozzle exit in one direction is representative of the entire plane.

References

1. W. W. Smith, et al, "Low Power Hydrazine Arcjet Qualification," IEPC Paper 91-148, Oct. 1991.

2. C. E. Vaughan, and R. J. Cassady, "An Updated Assessment of Electric Propulsion Technology for Near-Earth Space Missions," Paper AIAA- 92-3202, July 1992.

3. J. A. Pobst, I. J. Wysong, R.A. Spores, "Laser Induced Fluorescence of Ground State Hydrogen Atoms at Nozzle Exit of an Arcjet Thruster," AIAA

Paper AIAA-95-1973, 26th Plasmadynamics and Lasers Conference, 19-22 June, 1995, San Diego, California.

4. D. Keefer, D. Burtner, T. Moeller, and R. Rhodes, "Multiplexed Laser Induced Fluorescence and Non-Equilibrium Processes in Arcjets," Paper AIAA-94-2656, 25th Plasmadynamics and Lasers Conference, 20-23 July, 1994, Colorado Springs, Colorado.

5. G.W. Butler, I. D. Boyd, and M. A Cappelli, "Non-Equilibrium Flow Phenomena in Low Power Hydrogen Arcjets," Paper AIAA-95-2819, 31st Joint Propulsion Conference, 10-12 July, 1995, San Diego, California.

6. V. Babu, S.M. Aithal, and V.V. Subramaniam, "Propellant Internal Mode Dis-equilibrium and Frozen flow Losses in arcjets," Paper AIAA-94-2655, 25th Plasmadynamics and Lasers Conference, 20-23 July, 1994, Colorado Springs, Colorado.

7. S. Miller and M. Martinez-Sanchez, "Nonequilibrium Numerical Simulation of Radiation -Cooled Arcjet Thrusters," Paper IEPC-93-218, 23rd International Electric Propulsion Conference, 13-16, September, 1993, Seattle, Washington

8. T.W. Megli, H. Krier, R.L. Burton, and A. E. Mertogul, "Two Temperature Modeling of N_2/H_2 Arcjets," Paper AIAA-94-2413, 25th Plasmadynamics and Lasers Conference, 20-23 July, 1994, Colorado Springs, Colorado.

9. I. D. Boyd, private communication. Other results from the same model are included as part of G.W. Butler, I. D. Boyd, and M. A Cappelli, "Non-Equilibrium Flow Phenomena in Low Power Hydrogen Arcjets," Paper AIAA-95-2819, 31st Joint Propulsion Conference, 10-12 July, 1995, San Diego, California.

10. D. R. Beattie and M. A. Cappelli, "Molecular Hydrogen Raman Scattering in a Low Power Arcjet Thruster," Paper AIAA-92-3566, 28th Joint Propulsion Conference, 6-8 July, 1992, Nashville, Tennessee.

11. D. R. Beattie and M. A. Cappelli, "Raman Scattering Measurements of Molecular Hydrogen in an Arcjet Thruster Plume," Paper AIAA-95-1956, 26th Plasmadynamics and Lasers Conference, 19-22 June, 1995, San Diego, California.

12. J.E. Pollard, "Arcjet diagnostics by XUV Absorption Spectroscopy," Paper AIAA-92-2966, 23rd Plasmadynamics and Lasers Conference, 6-8 July, 1992, Nashville, Tennessee.

13. D.H. Manzella and M.A. Cappelli, "Vacuum Ultraviolet Absorption in a Hydrogen Arcjet," Paper AIAA-92-3564, 23rd Plasmadynamics and Lasers Conference, 6-8 July, 1992, Nashville, Tennessee.

14. D.A. Erwin, G.C. Pham-Van-Diep, and W.D. Deininger, "Laser-induced Fluorescence Measurements of Flow Velocity in High-Power Arcjet Thruster Plumes," AIAA J. 29, 1298 (1991).

15. J.G. Liebeskind, R.K. Hanson, and M.A. Cappelli, "Laser-induced Fluorescence Diagnostic for Temperature and Velocity Measurements in a Hydrogen Arcjet Plume," Appl. Optics 32, 6117 (1993).

16. J.E.M. Goldsmith, "Multiphoton-excited fluorescence measurements of atomic hydrogen in low-pressure flames," Proceedings of the 22nd Symposium (International) on Combustion, Combustion Institute, 1403 (1988); J.E.M. Goldsmith, "Two-step saturated fluorescence detection of atomic hydrogen in flames," Opt. Lett. 10, 116 (1985); J.E.M Goldsmith, J.A.Miller, R.J.M. Anderson, and L.R. Williams, "Multiphoton-excited fluorescence measurements of absolute concentration profiles of atomic hydrogen in low-pressure flames," Proceedings of the 23rd Symposium (International) on Combustion, Combustion Institute, 1821 (1990).

17. B.L Preppernau, D.A. Dolson, R.A. Gottscho, and T.A. Miller, "Temporally resolved laser diagnostic measurements of atomic hydrogen concentrations in RF plasma discharges," Plasma Chem. and Plasma Proc. 9, 157 (1989).

18. J. Bittner, K. Kohse-Hoinghaus, U. Meier, S. Kelm, and T.H. Just, "Determination of Absolute H Atom Concentrations in Low-Pressure Flames by Two-Photon Laser-Excited Fluorescence," Combustion and Flame 71, 41-50 (1988).

19. U. Meier, K. Kohse-Hoinghaus, and Th. Just, "H and O atom detection for combustion applications: study of quenching and laser photolysis effects," Chem. Phys. Lett. 126, 567 (1986); U. Meier, K. Kohse-Hoinghaus, L. Schafer, and C.-P. Klages, "Two-photon excited LIF determination of H-atom concentrations near a heated filament in a low-pressure H_2 environment," Appl. Opt. 29, 4993 (1990).

20. A. D. Tserepi, J. R. Dunlop, B. L. Preppernau, and T. A. Miller, "Absolute H-atom Concentration Profiles

in Continuous and Pulsed RF Discharges," J. Appl. Phys. 72, No. 7, 2638 (1992).

21. F.M. Curran and T.W. Haag, "An Extended Life and Performance Test of a Low Power Arcjet," Paper AIAA-88-3106, 24th Joint Propulsion Conference, 1988, New York, New York.

22. P.V. Storm and M.A. Cappelli, "High Spectral Resolution Emission Study of a Low Power Hydrogen Arcjet Plume," Paper AIAA 95-1960, 26th Plasmadynamics and Lasers Conference, 19-22 June, 1995, San Diego, California.

23. W. H. Press, B. P. Flannery, S. A. Teukolsky, and W. T. Vetterling, *Numerical Recipes: The Art of Scientific Computing*, 1st ed., Cambridge Univ. Press, Cambridge, 1986.

24. N. Georgiev, K. Nyholm, R. Fritzon, and M. Alden, "Developments of the amplified stimulated emission technique for spatially resolved species detection in flames," Optics Comm. 108, 71-76 (1994).

25. M.S. Brown and J.B. Jeffries, "Measurement of atomic concentrations in reacting flows through use of stimulated gain or loss," Applied Optics 34, 1127 (1995).

26. J.E.M. Goldsmith, "Two-photon-excited stimulated emission from atomic hydrogen in flames," J. Opt. Soc. Am. B 6, 1979 (1989).

27. C.R. Vidal, J. Cooper, and E.W. Smith, "Hydrogen Stark-broadening tables," Astrophys. J. Suppl. No. 214, vol. 25, 37-136 (1973).

28. D.J. Bamford, L.E. Jusinski, and W.K. Bischel, "Absolute two-photon absorption and three-photon ionization cross sections for atomic oxygen," Phys. Rev A 34, 185-198 (1986).

29. W. Demtröder, *Laser Spectroscopy, Basic Concepts and Instrumentation,* 3rd Printing, Springer-Verlag, Berlin, 1988.

30. P. V. Storm and M. A. Cappelli, "High Spectral Resolution Emission Study Of A Low Power Hydrogen Arcjet Plume," Paper AIAA-95-1960, 26th Plasmadynamics and Lasers Conference, 19-22 June, 1995, San Diego, California.

31. G. W. Butler, private communication.

32. T. Megli, Ph. D. Thesis, "A Nonequilibrium Plasmadynamics Model for Nitrogen/Hydrogen Arcjets," University of Illinois at Urbana-Champaign, 1995

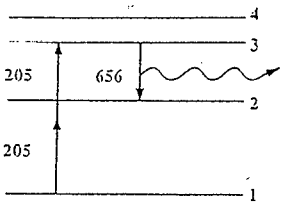

Figure 1. Energy level schematic (not to scale) of the hydrogen atom, showing the 2PLIF diagnostic technique.

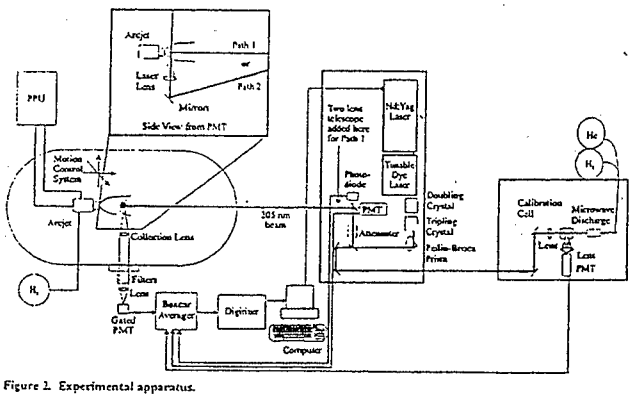

Figure 2. Experimental apparatus.

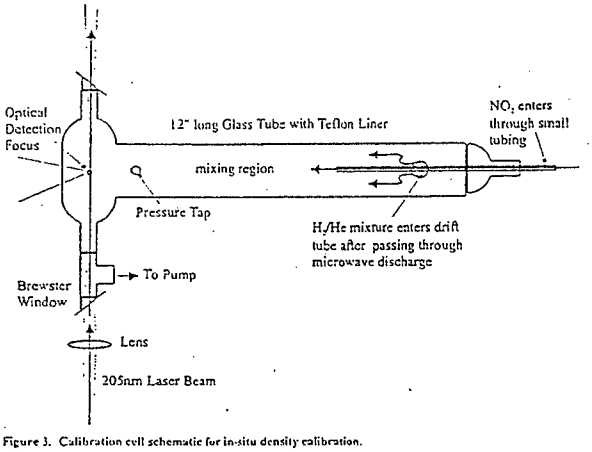

Figure 3. Calibration cell schematic for in-situ density calibration.

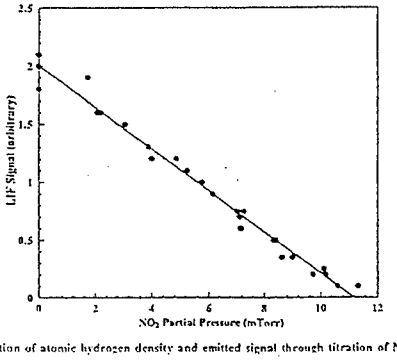

Figure 4. Determination of atomic hydrogen density and emitted signal through titration of NO_2 into calibration cell.

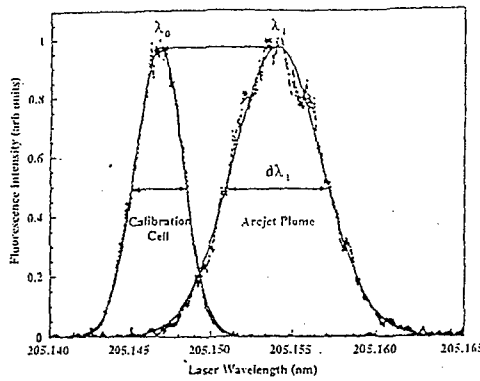

Figure 5. Sample 2PLIF spectrum of the hydrogen atom, showing the calibration signal from the discharge cell and the signal from the arcjet plume.

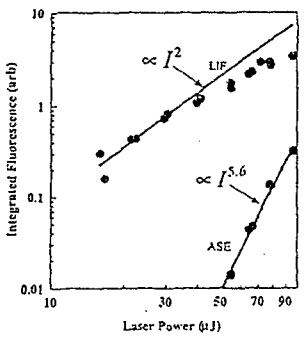

Figure 6. Arcjet study of LIF signal dependence on laser power compared to ASE power dependence, which has a much sharper response to laser power.

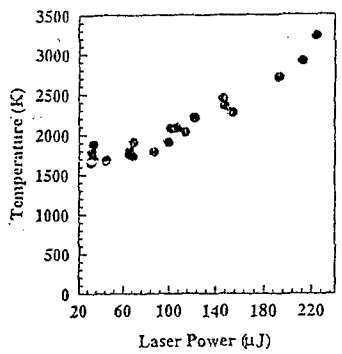

Figure 7. Apparent temperature for the arcjet at changing laser powers

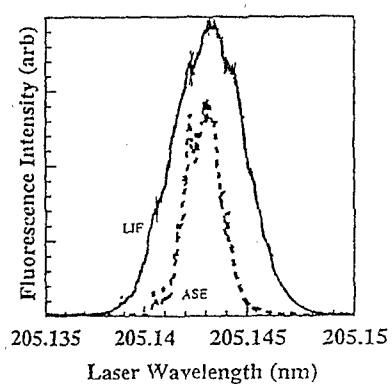

Figure 8. Narrower ASE spectrum compared with LIF spectrum.

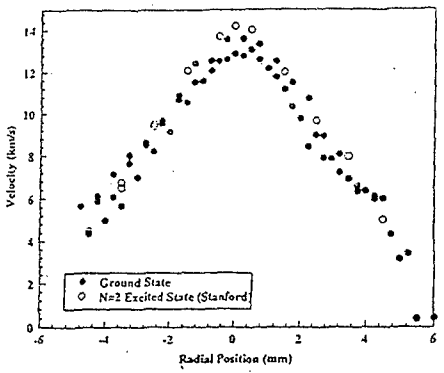

Figure 9. Profile across nozzle exit plane (0.4 mm from exit) of the axial velocity component of the ground state hydrogen atoms containing data from several different days. For comparison, corresponding data (same arcjet conditions, same profile location) for LIF of the electronically excited hydrogen atoms from Stanford University.[10]

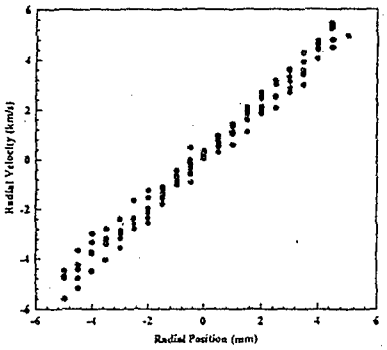

Figure 10. Profile across nozzle exit plane (0.4 mm from exit) of the radial velocity component of the ground state hydrogen atoms containing data from several different days where the radial position is measured parallel to the incoming laser beam.

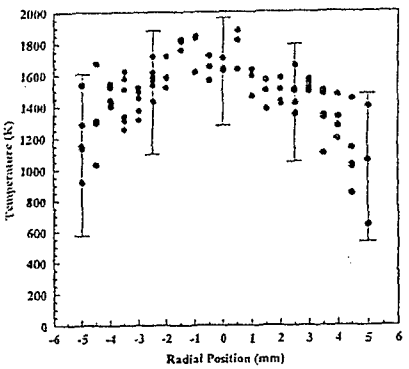

Figure 11. Profile across nozzle exit plane (0.4 mm from exit) of the translational temperature of the ground state hydrogen atoms containing data from two different days. The error bars are longer on the lower side to reflect the estimated amount of Stark broadening.

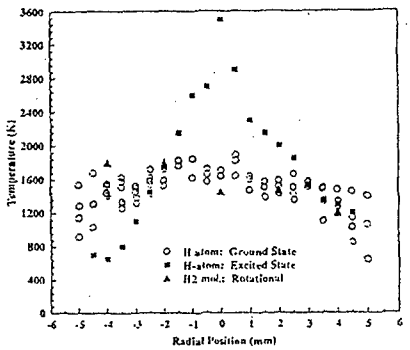

Figure 12. Temperature data shown in Figure 11, with corresponding data (same arcjet conditions, same profile location) for LIF of the electronically excited hydrogen atoms[10] and Raman molecular rotational temperatures,[11] both from Stanford University.

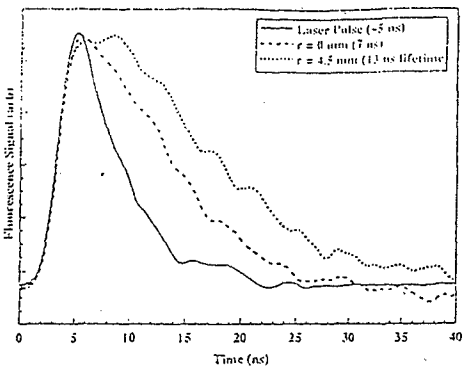

Figure 13. Fluorescence decay for n=3 hydrogen atoms at two positions along the arcjet nozzle exit plane. For comparison, a trace of the laser pulse alone (with no hydrogen atoms present) is shown.

	Arcjet Models (~1.4 kW, Hydrogen)			Arcjet Experiments (~1.4 kW, Hydrogen)	
Author	Butler[30]	Megli, Krier, and Burton[31]	Boyd[9]	Pobst, Wysong, and Spores	Beattie and Cappelli[32]
Affiliation	Olin Aerospace	University of Illinois	Cornell University	Phillips Laboratory	Stanford University
Specific Energy (MJ/kg)	100	105	100	105	100
H atom density (cm^{-3}) – nozzle exit / center	9.3×10^{14}	1.2×10^{15}	3.6×10^{14}	~1×10^{16} (Mach/Pitot/LIF)	---
H_2 density (cm^{-3}) – nozzle exit / center	8.5×10^{15}	7×10^{15}	8.2×10^{15}	---	~5×10^{15} (Raman Scattering)
Molecular Dissociation Fraction	5%	8%	18%	~50%	

Table 1. Listing of atomic and molecular density data near the center of the 1kW class arcjet nozzle exit for three modeling and two experimental efforts.

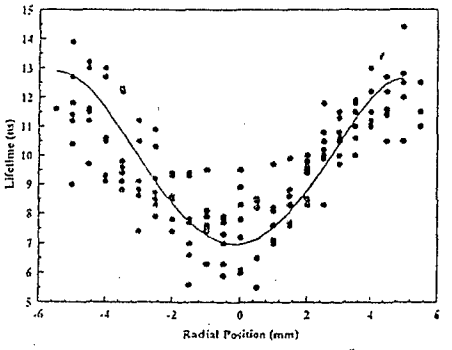

Figure 14. Fluorescence lifetimes as a function of position along nozzle exit from many different days. The line represents a best fit to the data.

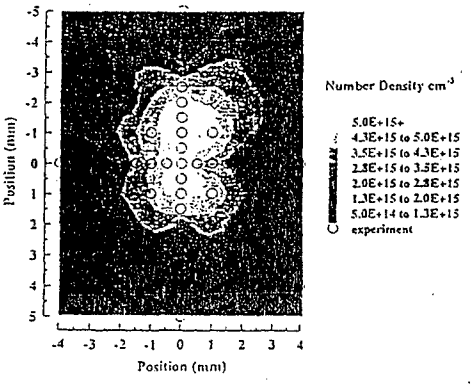

Figure 17. Two dimensional profile near the arcjet exit plane of the absolute number density of ground state hydrogen atoms.

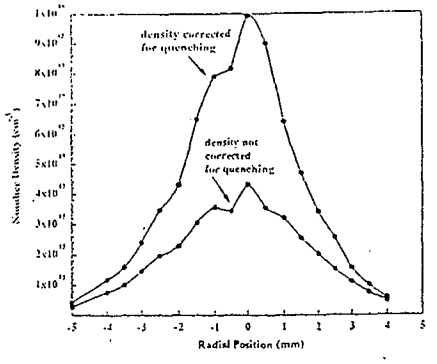

Figure 15. Significance in correcting for quenching when determining density from a relative fluorescence profile. Note that the largest correction occurs in the center of the profile where the quenching is greatest and is minimal at the edges where quenching is relatively insignificant.

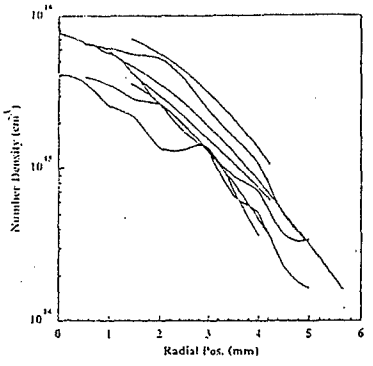

Figure 18. Representation of each "spoke" of data taken in Figure 17 vs. distance from center.

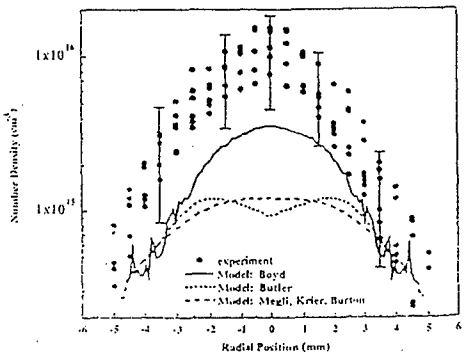

Figure 16. Profile across nozzle exit plane (0.4 mm from exit) of the absolute number density of ground state hydrogen atoms containing data from two different days. Shown for comparison are the predictions for number density profile from computational arcjet models.[9,30,31]

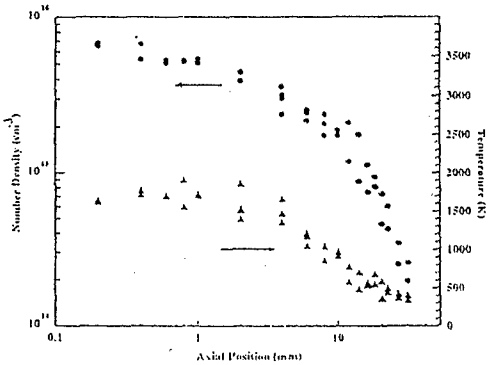

Figure 19. Centerline density and temperature data taken axially from the nozzle exit. The position scale is shown logarithmically to emphasize the gradients near the nozzle exit.